Title
Quantum phase transition in a multiconnected Jaynes-Cummings lattice

Author
Tian, Lin

Publication Date
2017-11-07

Peer reviewed

Quantum phase transition in a multiconnected Jaynes-Cummings lattice

Jian Xue,[1,2] Kangjun Seo,[3] Lin Tian,[3,*] and Tao Xiang[1,4,†]
[1]*Institute of Physics, Chinese Academy of Sciences, Beijing 100190, China*
[2]*University of Chinese Academy of Sciences, Beijing 100049, China*
[3]*School of Nature Sciences, University of California, Merced, California 95343, USA*
[4]*Collaborative Innovation Center of Quantum Matter, Beijing 100190, China*
(Received 7 February 2017; published 7 November 2017)

The rapid progress in quantum technology enables the implementation of artificial many-body systems with correlated photons and polaritons. A multiconnected Jaynes-Cummings (MCJC) lattice can be constructed by connecting qubits and cavities alternately. Such models can be realized with superconducting qubits coupled to superconducting microwave resonators or with quantum dots coupled to optical nanocavities. We study the physical properties of a one-dimensional MCJC lattice using the density-matrix renormalization-group method. This model has an intrinsic symmetry between the left and right qubit-cavity couplings. The competition between these couplings may drive the ground state either to a Mott-insulating phase or to a superfluid phase at integer fillings. We calculate the single-particle and density-density correlation functions, the correlation lengths in the Mott-insulating phase, and the Luttinger parameters in the superfluid phase and determine accurately the critical points that separate these two phases.

DOI: 10.1103/PhysRevB.96.174502

I. INTRODUCTION

The past few decades have witnessed enormous progress in the development of quantum devices in various physical systems, such as superconducting devices, trapped ions, and semiconductor photonic devices, with significant improvement in their controllability and coherent property [1–4]. Besides the goal of building scalable fault-tolerant quantum computers [5], these devices have been exploited to emulate numerous many-body phenomena that are difficult to solve with conventional techniques [6–10] in condensed-matter physics, high-energy physics, and nonequilibrium systems [11–26]. In particular, rich varieties of many-body effects in ultracold atoms coupled to optical cavities have been intensively studied in recent theoretical and experimental works [27–35].

Meanwhile, the construction of artificial many-body systems leads to the study of strongly correlated photons and polaritons [36,37]. In the coupled-cavity array (CCA) models [38–40], photons can hop between adjacent cavities. The cavity modes are also coupled to a nonlinear medium, such as qubits and defects, which adds nonlinearity to the spectrum of the polariton excitations. The nonlinearity can be viewed as an on-site Hubbard interaction, in comparison to the Bose-Hubbard model [41–44]. The competition between the hopping and the nonlinearity results in quantum phase transitions between the Mott-insulating (MI) phase with localized polariton excitations and the superfluid (SF) phase with long-range spatial correlation. In the past few years, the CCA has been studied extensively in theory and in experiments [45–53]. Photon blockade has been demonstrated in a recent experiment [54]. Dynamical quantum phase transition with driven and dissipative cavities has been investigated [55,56]. In recent works [57–60], a multiconnected Jaynes-Cummings (MCJC) lattice was introduced, where qubits and cavities are connected alternately. Both CCA and MCJC can be realized with the microwave modes in superconducting resonators coupled to superconducting qubits or with optical modes in nanocavities coupled to quantum dots or defects [1,3]. A specific realization of the MCJC lattice is to connect Xmon qubits to superconducting resonators, enabled by the rich connectivity of superconducting circuits [61,62]. Different from the CCA, no direct coupling exists between cavities in the MCJC. Quantum phase transition in a MCJC lattice has been studied with exact diagonalization [57,58]. It was shown that at integer filling, transitions between the MI and SF phases occur due to the competition between the qubit-cavity couplings. These systems provide a promising platform to study correlations in interacting photons and polaritons.

In this paper, we study the quantum critical behavior of the one-dimensional (1D) MCJC model using the density-matrix renormalization group (DMRG) [63,64]. This method has previously been used to study the Bose-Hubbard and CCA models [43–45,52]. We calculate the polariton ground states at both integer and half fillings. The phase boundaries separating the MI and SF phases are obtained by calculating the chemical potentials [65]. The single-particle density matrix is utilized to obtain the correlation lengths and the Luttinger parameters of the qubits and the cavities. Using the Luttinger parameters extrapolated to the thermodynamic limit, the quantum critical points are determined accurately and compared with the previous results [57,58]. We also calculate the structure factors and find no evidence for a crystalline or charge-density-wave (CDW) phase at half filling. Our result could shed light on the studies of many-body effects in strongly correlated photons and polaritons.

This paper is organized as follows. In Sec. II, we introduce the MCJC model and discuss its relation to the well-studied Bose-Hubbard model. In Sec. III, we describe the DMRG method for the MJCJ model and discuss the results for entanglement entropy and local density. In Sec. IV, the DMRG results for the phase boundary, single-particle density matrix,

*ltian@ucmerced.edu
†txiang@iphy.ac.cn

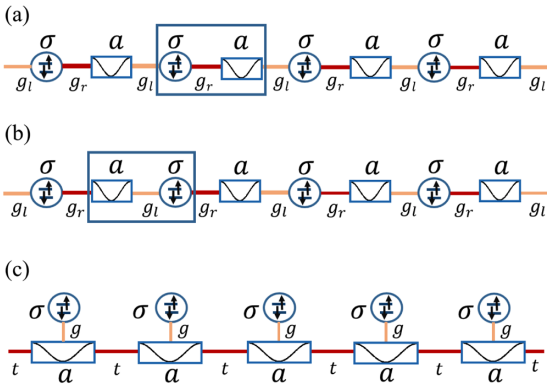

FIG. 1. Schematic of (a) and (b) a 1D MCJC and (c) a CCA. The circles represent the qubits, and the blocks represent the cavities. A unit cell of the MCJC consists of a qubit and an adjacent cavity coupled to the qubit via (a) g_r or (b) g_l.

correlation lengths, Luttinger parameters, and density-density correlation functions are discussed. Conclusions are given in Sec. V.

II. MULTICONNECTED JAYNES-CUMMINGS LATTICE

A. Model Hamiltonian

A MCJC lattice is composed of alternately connected qubits and cavities [57,58]. A schematic of a 1D MCJC lattice is shown in Fig. 1, where each qubit couples to two adjacent cavities. The Hamiltonian of this model reads ($\hbar = 1$)

$$H_t = H_0 + H_l + H_r, \tag{1}$$

$$H_0 = \sum_i \left(\frac{\omega_z}{2}\sigma^z_{2i-1} + \omega_c a^\dagger_{2i} a_{2i}\right), \tag{2}$$

$$H_l = \sum_i g_l\left(\sigma^+_{2i-1}a_{2i-2} + a^\dagger_{2i-2}\sigma^-_{2i-1}\right), \tag{3}$$

$$H_r = \sum_i g_r\left(\sigma^+_{2i-1}a_{2i} + a^\dagger_{2i}\sigma^-_{2i-1}\right), \tag{4}$$

where ω_z is the energy splitting of the qubits, ω_c is the frequency of the cavity modes, $\sigma_i^{z,+,-}$ are the Pauli matrices, a_i is the annihilation operator of the cavity modes, g_l (g_r) is the coupling constant between a qubit and a cavity next to it from the left- (right-) hand side. In this paper, periodic boundary conditions are assumed.

Similar to the CCA model [Fig. 1(c)], a unit cell contains one qubit and one cavity. But unlike in the CCA model, the cavities are not directly coupled to each other. The unique geometry of this model renders a symmetry between g_l and g_r, and the energy spectrum is unchanged under the exchange of these two coupling constants. This leads to the symmetry in the phase diagram discussed below.

The MCJC model can be realized with superconducting quantum circuits, in particular the Xmon or gmon qubits, where controllable couplings between qubits and cavities have been achieved [61,62]. The couplings in such systems can be tuned continuously from zero to a few hundred megahertz, which makes it an ideal system for studying strongly correlated effects of polaritons [57,60,66]. In the discussion below, we set the coupling constants $g_{l,r}/2\pi \in (0,300)$ MHz, $\omega_c/2\pi = 10$ GHz, and $\omega_z = \omega_c$ ($\Delta = 0$). These parameters can be reached with current experimental technology. Recent progress in superconducting quantum devices also ensures long decoherence times for qubits and resonators. The decoherence times of Xmon or gmon qubits can easily exceed 10 μs. For a superconducting resonator with a 10-GHz frequency and a quality factor of 10^5, the relaxation time of resonator states with several photons is $\sim$2 μs. In comparison, quantum manipulation or preparation of qubit and resonator states can be achieved within 10 ns [17,18,67]. With the time for state preparation much shorter than the decoherence times, our system can be prepared and can remain in a ground state with a finite number of polariton excitations without being strongly affected by qubit decoherence or resonator dissipation.

The energy spectrum of a single unit cell in the MCJC lattice can be exactly solved. If we take a qubit with its right cavity as a unit cell [Fig. 1(a)], the Hamiltonian of the ith unit cell is given by

$$H_i = \omega_c a^\dagger_{2i} a_{2i} + \frac{\omega_z}{2}\sigma^z_{2i-1} + g_r(a^\dagger_{2i}\sigma^-_{2i-1} + \sigma^+_{2i-1}a_{2i}), \tag{5}$$

which is nothing but the standard Jaynes-Cummings (JC) model between a qubit and a cavity [68]. It has been extensively studied in cavity and circuit quantum electrodynamic (QED) systems [69–71]. In the ground state, there is no photon excitation, and the qubit is in the down-spin state. If we use $|n,\sigma\rangle$ to denote the basis states, then the ground state is given by $|0,\downarrow\rangle$, where n is the number of photons in the cavity and $\sigma = (\uparrow,\downarrow)$ corresponds to the two spin states of the qubit, with ground-state energy $E_0 = -\omega_z/2$. The higher excitation states appear in pairs and can be regarded as a doublet, resulting from the coupling between the basis states $|n-1,\uparrow\rangle$ and $|n,\downarrow\rangle$. In this doublet subspace, the Hamiltonian can be expressed as a 2×2 matrix,

$$[H_i]_n = \begin{pmatrix} (n-1)\omega_c + \frac{\omega_z}{2} & \sqrt{n}g_r \\ \sqrt{n}g_r & n\omega_c - \frac{\omega_z}{2} \end{pmatrix}. \tag{6}$$

There is no coupling between different doublets. Diagonalizing this matrix, we obtain the eigenstates

$$|n,\pm\rangle = \gamma_{n\pm}|n,\downarrow\rangle + \rho_{n\pm}|n-1,\uparrow\rangle, \tag{7}$$

where $\gamma_{n+} = -\rho_{n-} = \sin\theta_n$, $\gamma_{n-} = \rho_{n+} = \cos\theta_n$, and

$$\theta_n = \arctan\left(\frac{\sqrt{4ng_r^2 + \Delta^2} - \Delta}{2\sqrt{n}g_r}\right). \tag{8}$$

In the notation $|n,\pm\rangle$, $n = \langle\sigma^+_{2i-1}\sigma^-_{2i-1} + a^\dagger_{2i}a_{2i}\rangle$ refers to the total number of excitations in the unit cell. The corresponding eigenenergies are

$$E_{n,\pm} = \left(n - \frac{1}{2}\right)\omega_c \pm \frac{1}{2}\sqrt{4ng_r^2 + \Delta^2}, \tag{9}$$

where $\Delta = \omega_z - \omega_c$ is the detuning between the qubit and the cavity. At $\Delta = 0$, the doublets become

$$|n,\pm\rangle = \frac{1}{\sqrt{2}}|n,\downarrow\rangle \pm \frac{1}{\sqrt{2}}|n-1,\uparrow\rangle, \tag{10}$$

and $E_{n,\pm} = (n-1/2)\omega_c \pm \sqrt{n}g_r$.

B. Polariton representation

To analyze the MCJC model at finite g_l, we adopt the polariton mapping technique [40,49] and define a polariton operator at each unit cell,

$$p^i_{n\alpha} \equiv |0,-\rangle_i \langle n,\alpha|. \tag{11}$$

This is an operator to annihilate an n-polariton state at the ith unit cell. These operators satisfy the commutation relation

$$\left[p^i_{n\alpha}, p^{j\dagger}_{m\beta}\right] = \delta_{ij}(\delta_{n\alpha,m\beta}|0,-\rangle_i\langle 0,-| - |m,\beta\rangle_i\langle n,\alpha|). \tag{12}$$

Using these operators, the spin and photon operators can be expressed as

$$a_i = \sum_{n,\alpha,\alpha'} t^n_{\alpha\alpha'} p^{i\dagger}_{(n-1)\alpha'} p^i_{n\alpha}, \tag{13}$$

$$\sigma^-_i = \sum_{n,\alpha,\alpha'} k^n_{\alpha\alpha'} p^{i\dagger}_{(n-1)\alpha'} p^i_{n\alpha}, \tag{14}$$

where the coefficients are given by

$$t^n_{\alpha\beta} = \sqrt{n}\gamma_{n\alpha}\gamma_{(n-1)\beta} + \sqrt{n-1}\rho_{n\alpha}\rho_{(n-1)\beta} \tag{15}$$

and $k^n_{\alpha\alpha'} = \rho_{n\alpha}\gamma_{(n-1)\alpha'}$.

The Hamiltonian H_t can be represented in terms of the polariton operators. For example, at $\Delta = 0$,

$$H_t = \sum_{i\alpha n}[(n-1/2)\omega_c + \alpha\sqrt{n}g_r]p^{i\dagger}_{n\alpha}p^i_{n\alpha} + g_l\sum_{inm}\sum_{\alpha\alpha'\beta\beta'} k^n_{\alpha\alpha'}t^m_{\beta\beta'}V^{\alpha\alpha'\beta\beta'}_{imn}, \tag{16}$$

with a hopping term

$$V^{\alpha\alpha'\beta\beta'}_{imn} = p^{i\dagger}_{n\alpha}p^{(i-1)\dagger}_{(m-1)\beta'}p^{i-1}_{m\beta}p^i_{(n-1)\alpha'} + \text{H.c.} \tag{17}$$

The first term in Eq. (16) describes the local polariton states with a nonlinear spectrum that resembles the effective on-site interactions. The second term in Eq. (16) describes the hopping of a polariton from site $(i-1)$ (reducing the number of polaritons from m to $m-1$) to site i (increasing the number of polaritons from $n-1$ to n). The competition between these two terms leads to a transition between the MI and SF phases. When $g_l = 0$, the system is in the MI phase. Increasing g_l, especially in the parameter range where g_l becomes comparable to g_r, the hopping can effectively lower the on-site interaction generated by double occupancy and drive the system into the SF phase at a critical point $g_l/g_r = \beta_0$. This is similar to the MI-SF phase transition in the Bose Hubbard model with the increase of the hopping integral [44]. In the SF phase, the low-energy excitations of interacting polaritons can be described by the Luttinger liquid Hamiltonian [72,73]. Parameters in the Luttinger liquid Hamiltonian determine the exponents of the correlation functions. When further increasing g_l, another MI phase whose properties are similar to the first one by simply exchanging g_l with g_r emerges above a critical point $g_l/g_r = 1/\beta_0$. This analysis agrees with the result obtained by an exact diagonalization calculation [57].

The polariton mapping is valid in the limits of $g_l \ll g_r$ and $g_r \ll g_l$, when the two couplings are significantly different from each other. In these limits, the system is dominated by the stronger one of these two couplings and can be described with the polariton eigenmodes in each unit cell.

C. Equivalence to the Bose-Hubbard model

In the low-energy limit, the MCJC is equivalent to the Bose-Hubbard model. Below we give a proof for this. Consider the Bose-Hubbard model with the Hamiltonian

$$H_{BH} = \sum_i\left[-t(b^\dagger_i b_{i-1} + \text{H.c.}) - \mu b^\dagger_i b_i + \frac{U}{2}n_i(n_i-1)\right], \tag{18}$$

where b_i ($b^\dagger_i$) is the annihilation (creation) operator of bosons at site i, U is the on-site Hubbard interaction, t is the hopping integral, and μ is the chemical potential. By introducing a polaritonlike operator

$$p^i_n = |0\rangle_i\langle n|, \tag{19}$$

we can represent the boson operator as

$$b_i = \sum_n \sqrt{n}|n-1\rangle_i\langle n| = \sum_n \sqrt{n}p^{i\dagger}_{n-1}p^i_n. \tag{20}$$

These p operators satisfy the commutation relation

$$\left[p^i_n, p^{j\dagger}_m\right] = \delta_{ij}(|0\rangle_i\langle 0|\delta_{n,m} - |m\rangle_i\langle n|). \tag{21}$$

In this new representation, the Bose-Hubbard model becomes

$$H_{BH} = \sum_{in}\left[-\mu n + \frac{U}{2}n(n-1)\right]p^{i\dagger}_n p^i_n - t\sum_{imn}\sqrt{mn}\tilde{V}_{imn}, \tag{22}$$

where

$$\tilde{V}_{imn} = p^{i\dagger}_n p^{(i-1)\dagger}_{m-1}p^{i-1}_m p^i_{n-1} + \text{H.c.} \tag{23}$$

By comparing Eq. (16) with Eq. (22), we find that in the low-energy limit where the contribution from the higher-polariton excitations is negligible, the MCJC is equivalent to the Bose-Hubbard model if the parameters of these two models are related by

$$\left(n-\tfrac{1}{2}\right)\omega_c - \sqrt{n}g_r \to -\mu n + \tfrac{1}{2}Un(n-1), \tag{24}$$

$$g_l k^n_{--}t^m_{--} \to -t\sqrt{mn}. \tag{25}$$

We can also determine the effective Hubbard interaction in the MCJC by directly comparing the energies of the low-energy excitations in these two models. In the MCJC lattice, the lowest energy to excite one polariton is $\Delta E_1 = E_{1,-} - E_0$, and the energy to add the second polariton is $\Delta E_2 = E_{2,-} - E_{1,-}$. In the limit $\Delta = 0$, $\Delta E_1 = \omega_c - g_r$ and $\Delta E_2 = \omega_c - (\sqrt{2}-1)g_r$. For the Bose-Hubbard model, the corresponding energies are $\Delta E_1 = E_1 - E_0 = -\mu$ and $\Delta E_2 = E_2 - E_1 = -\mu + U$. By setting these two excitation energies equal in these two models, we find that the effective on-site interaction $U = (2-\sqrt{2})g_r$ for the lowest states in the MCJC at $\Delta = 0$. Similarly, at $\Delta = 0$, $\gamma_+ = -\rho_- = \sqrt{2}/2$, $\gamma_- = \rho_+ = \sqrt{2}/2$, $t_{\alpha\beta} = \sqrt{n}/2 + \alpha\beta\sqrt{n-1}/2$, and $k_{\alpha\beta} = \alpha/2$. From Eq. (25), we obtain the effective hopping amplitude $t = g_l/4$.

D. Integer and noninteger fillings

The total number of polaritons in the entire lattice

$$N_t = \sum_i (\sigma^+_{2i-1}\sigma^-_{2i-1} + a^\dagger_{2i} a_{2i}) \tag{26}$$

is a conserving operator. It commutes with the model Hamiltonian, $[N_t, H_t] = 0$.

At an integer filling, $N = \langle N_t \rangle$ is an integer multiple of the number of unit cells L. In the limit $g_l = 0$, the unit cells are decoupled, and the ground state is a product state with all the unit cells being in the lower polariton states $|1,-\rangle$, and the corresponding energy is $E = NE_{1,-}$. We denote this state as $|1111\ldots\rangle$ and the empty site as $|0\rangle$ for simplicity. Apparently, this state is in the MI phase, and there is a finite energy gap for adding or removing one polariton excitation from the system.

With finite g_l, the polariton excitations can tunnel between adjacent unit cells. The competition between the tunneling and the effective on-site repulsion strongly affects the physical properties of this model.

Away from integer filling, the ground states become highly degenerate. For example, in a lattice of $L = 4$ at half filling, i.e., $N = 2$, the ground states are sixfold degenerate, with the following polariton configurations: $|1010\rangle$, $|0101\rangle$, $|1100\rangle$, $|0110\rangle$, $|0011\rangle$, and $|1001\rangle$. In the weak intercell coupling limit, $g_l \ll g_r$, we can treat H_l as a perturbation. In the first-order approximation, the perturbed Hamiltonian can be expressed in this sixfold-degenerate subspace as

$$H_l = -\frac{g_l}{2}\begin{pmatrix} 0 & 0 & 1 & 1 & 1 & 1 \\ 0 & 0 & 1 & 1 & 1 & 1 \\ 1 & 1 & 0 & 0 & 0 & 0 \\ 1 & 1 & 0 & 0 & 0 & 0 \\ 1 & 1 & 0 & 0 & 0 & 0 \\ 1 & 1 & 0 & 0 & 0 & 0 \end{pmatrix}. \tag{27}$$

By diagonalization, we obtain the ground state

$$|g\rangle = \frac{\sqrt{2}}{4}(|1100\rangle + |0110\rangle + |0011\rangle + |1001\rangle) + \frac{1}{2}(|1010\rangle + |0101\rangle), \tag{28}$$

and the corresponding correction to the ground-state energy $E^{(1)} = -\sqrt{2}g_l$.

III. THE DMRG METHOD

We use the finite-lattice algorithm of the DMRG to characterize the critical behavior of the MCJC model [63]. This method has already been used to study the critical behavior and quantum dynamics of low-dimensional strongly correlated systems, including the 1D Bose-Hubbard and CCA models [43–45,52]. In the calculation, we limit the number of photon excitations at each cavity to be less than or equal to five. For the cases we have examined, we find that this is a good approximation because the contribution from the states with more than five photons at one cavity to the ground-state energy is much smaller than the truncation error.

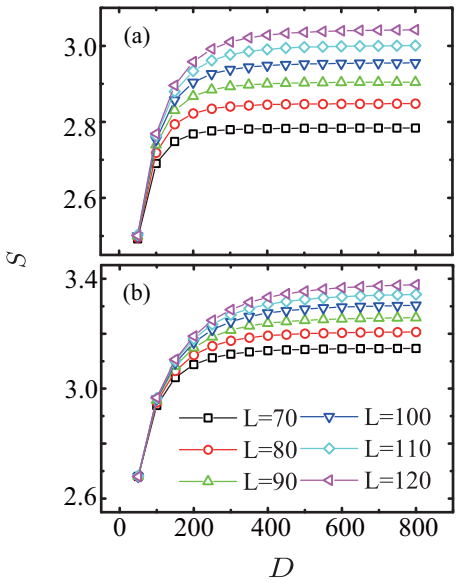

FIG. 2. The entanglement entropy S as a function of the bond dimension D for the MCJC at (a) half filling $N/L = 0.5$ and (b) integer filling $N/L = 1$, both with $g_{l,r}/2\pi = 150$ MHz.

In order to see how fast the DMRG calculations converge with the bond dimension D, which is the dimension of the truncated space during the iteration, we calculate the entanglement entropy of the ground state [74], defined by

$$S = -\mathrm{Tr}(\rho_L \ln \rho_L), \tag{29}$$

where ρ_L is the reduced density matrix for the left half of the lattice. Figure 2 shows the entanglement entropy as a function of the bond dimension D at both half and integer fillings at the symmetric point $g_l = g_r$. After a rapid increase at small D, we find that the entanglement entropy becomes almost saturated, which suggests that the ground-state wave function is converged, when D is larger than 500. To further ensure the convergence, we take $D = 600$ for all the calculations presented below.

For all the cases we have studied, we find that the ground states are translation invariant, as revealed by the distribution functions of the local excitation densities of qubits and cavities, defined by $\bar{n}^q_i = \langle \sigma^+_i \sigma^-_i \rangle$ and $\bar{n}^r_i = \langle a^\dagger_i a_i \rangle$, respectively. Our calculation indicates that the excitation densities are homogenous on the whole lattice with no obvious fluctuations. For example, for the system with $L = 120$ at the integer filling and $\Delta = 0$, we find that $\bar{n}^q_i = 0.40$ and $\bar{n}^r_i = 0.60$ when $g_{l,r}/2\pi = 150$ MHz and $\bar{n}^q_i = 0.46$ and $\bar{n}^r_i = 0.54$ when $g_l/2\pi = 55$ MHz and $g_r/2\pi = 245$ MHz on all the lattice sites. One interesting observation is that the difference $|\bar{n}^q_i - \bar{n}^r_i|$ between the qubit and cavity excitation densities in the limit of $g_l \ll g_r$ (and, similarly, $g_r \ll g_l$) is smaller than that at $g_l = g_r$. This is because in the limit $g_l \ll g_r$, the system behaves like a chain of uncoupled JC models where the excitation is equally split between the qubit and the cavity. However, at $g_l = g_r$, the polariton excitations can hop along the lattice, enlarging the splitting of local densities. A similar result is found at half filling.

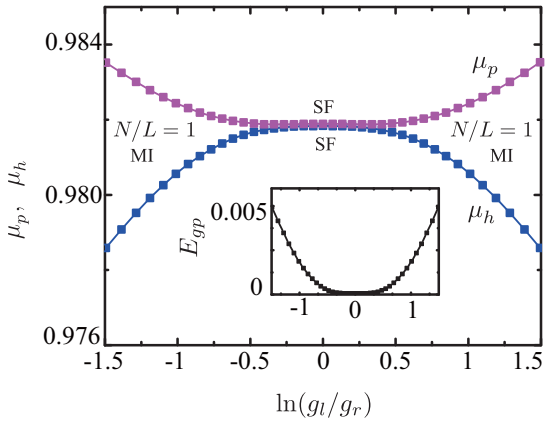

FIG. 3. The chemical potentials μ_p and μ_h versus $\ln(g_l/g_r)$ for the MCJC model at the integer filling $N/L = 1$ with $(g_r + g_l)/2\pi = 300$ MHz. Inset: the energy gap E_{gp} versus $\ln(g_l/g_r)$ at $N/L = 1$.

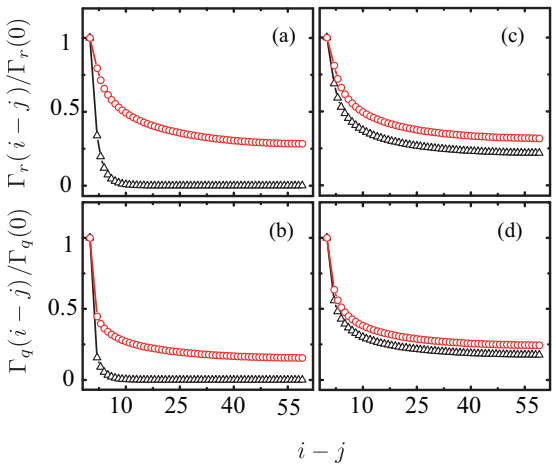

FIG. 4. The normalized single-particle density matrices $\Gamma_r(i-j)/\Gamma_r(0)$ and $\Gamma_q(i-j)/\Gamma_q(0)$ versus $(i-j)$ for the MCJC model with $L = 120$ at (a) and (b) integer and (c) and (d) half filling. Circles: $g_{l,r}/2\pi = 150$ MHz; triangles: $g_l/2\pi = 55$ MHz, $g_r/2\pi = 245$ MHz.

IV. NUMERICAL RESULTS

A. Phase boundaries

We calculate the ground-state energy $E_L(N)$ of the MCJC model with L unit cells and N polariton excitations using the DMRG. The chemical potential for adding or removing a polariton to the ground state is then determined by the formula

$$\mu_p(N,L) = E_L(N+1) - E_L(N), \tag{30}$$

$$\mu_h(N,L) = E_L(N) - E_L(N-1). \tag{31}$$

Here μ_p and μ_h are the chemical potentials for adding and removing a polariton, respectively [44]. To obtain the chemical potentials in the thermodynamic limit, we first calculate these quantities for finite-lattice systems with L up to 120 and then perform an extrapolation using the formula

$$\mu_\gamma(N,L) = \mu_\gamma + b_\gamma/L \quad (\gamma = p,h), \tag{32}$$

where μ_γ is the extrapolated chemical potential in the thermodynamic limit.

Figure 3 shows the extrapolated chemical potentials, μ_p and μ_h, as functions of $\ln(g_l/g_r)$. At the integer filling with $N = L$, we find that $\mu_p = \mu_h$ in the regime $g_l \sim g_r$ (small $|\ln(g_l/g_r)|$) within numerical errors. As the ratio $|\ln(g_l/g_r)|$ increases, a finite difference appears between μ_p and μ_h, corresponding to the opening of a finite-energy gap for adding or removing a polariton [44]. Thus there is a transition from the SF phase in the small $|\ln(g_l/g_r)|$ regime to the MI phase in the large $|\ln(g_l/g_r)|$ regime. In the SF phase, there is no gap in the energy spectrum, and $\mu_p = \mu_h$. However, in the MI phase, the energy to add or remove a polariton becomes different, and $\mu_p > \mu_h$. The extrapolated chemical potentials shown in Fig. 3 thus determine the phase boundaries that separate the MI and SF phases. If the chemical potential falls between μ_p and μ_h in the MI phase, the filling factor is fixed at $N/L = 1$, and the polariton density remains a constant within this phase with zero compressibility.

At integer filling, there are two quantum critical points which are symmetric with respect to the point $\ln(g_l/g_r) = 0$. The transitions between the MI and SF phases in this 1D system are of the Kosterlitz-Thouless (KT) type [72,73]. These transitions result from the competition between g_l and g_r. However, in the Bose-Hubbard and CCA models, the phase transitions are due to the competition between the hopping and the on-site interaction [38–41].

The inset of Fig. 3 shows the energy gap for exciting a polariton, $E_{gp} = \mu_p - \mu_h$, as a function of $\ln(g_l/g_r)$. It is clear that there is a finite regime in which $E_{gp} = 0$. As is well known, the transition between MI and SF phases in this system is driven by phase fluctuations, and the excitation gap can be written as $E_{gp} \sim \exp(-c/|\beta - \beta_0|)$, with $\beta = g_l/g_r$ and c being a dimensionless parameter. Using our numerical result, we fit these parameters to be $\beta_0 = 0.933$ and $c = 2.375$. Because the energy gap changes slowly with β near the critical points, this fitting is often inaccurate.

At half filling, the results of chemical potentials indicate that there is no difference in the energy for adding or removing a polariton, i.e., $\mu_p = \mu_h$, in the whole parameter regime. Thus there is no MI-SF phase transition, and the ground state is always in the SF phase.

B. Correlation functions

The single-particle density matrices for the qubits and cavities are defined, respectively, by

$$\Gamma_q(i-j) = \langle \sigma^+_{2i-1}\sigma^-_{2j-1}\rangle, \tag{33}$$

$$\Gamma_r(i-j) = \langle a^\dagger_{2i}a_{2j}\rangle. \tag{34}$$

They measure the correlations of polariton excitations [75,76].

Figure 4 shows the normalized single-particle density matrices $\Gamma_r(i-j)/\Gamma_r(0)$ and $\Gamma_q(i-j)/\Gamma_q(0)$ versus $i-j$ for two sets of parameters. At the integer filling, $N/L = 1$, both density matrices drop exponentially to zero with the increase of the distance between the two unit cells in the MI phase, $g_l/g_r \ll 1$. In the SF phase, however, the two density matrices remain finite even in the large-distance limit, indicating the

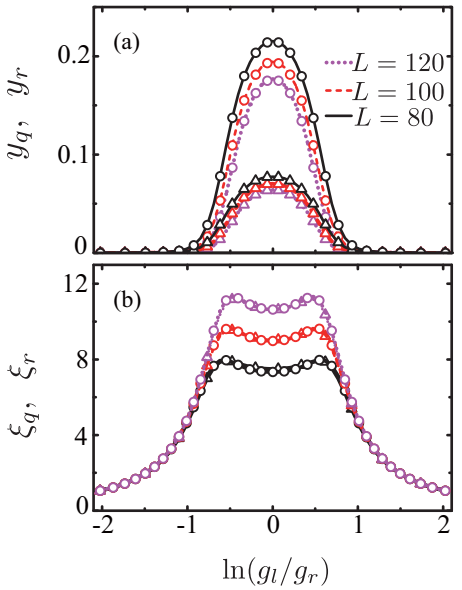

FIG. 5. (a) The coefficients y_q and y_r and (b) correlation lengths ξ_q and ξ_r versus $\ln(g_l/g_r)$ for the MCJC model with $L = 80,100,120$ and $(g_r + g_l)/2\pi = 300$ MHz. Circles: y_r and ξ_r; triangles: y_q and ξ_q.

existence of superfluid off-diagonal long-range order. At half filling, $N/L = 1/2$, the ground state is in the SF phase, and the two density matrices behave qualitatively similarly to the case of $g_l = g_r$ at the integer filling: they decrease with the increase of the distance between the two unit cells and saturate to certain finite values in the large-distance limit.

The single-particle density matrices can be fitted using the formulas

$$\Gamma_\alpha(i-j) = y_\alpha + A_q e^{-\frac{|i-j|}{\xi_\alpha}} \quad (\alpha = q,r), \tag{35}$$

where ξ_q (ξ_r) is the correlation length between two qubits (cavities). Figure 5(a) shows the coefficients y_q and y_r as functions of $\ln(g_l/g_r)$. As expected, both y_q and y_r are zero in the MI phase but become finite in the SF phase around the regime $\ln(g_l/g_r)$ close to zero.

The correlation lengths, shown in Fig. 5(b), increase quickly around the critical points in the MI phases. But we do not see the divergence of the correlation lengths at the critical point due to the finite-lattice-size effect. At the critical point, the entanglement entropy is expected to grow logarithmically with the system size. Thus in order to accurately determine the critical points from the divergent correlation lengths, we need to enlarge not just the lattice size but also the number of states retained in the DMRG calculation.

From the density-density correlation functions, we calculate the structure factors of the qubits ($\alpha = q$) and cavities ($\alpha = r$), defined by

$$S_\pi^\alpha = \frac{1}{N^2}\sum_{i,j}(-1)^{|i-j|}\langle n_i^\alpha n_j^\alpha\rangle \quad (\alpha = q,r), \tag{36}$$

where $n_i^r = a_i^\dagger a_i$ and $n_i^q = \sigma_i^+\sigma_i^-$. Figure 6 shows S_π^q and S_π^r as functions of $1/L$ at half filling with $g_l/2\pi = 55$ MHz and $g_r/2\pi = 245$ MHz. Within numerical errors, the extrapolated structure factors are found to be approximately zero, indicating

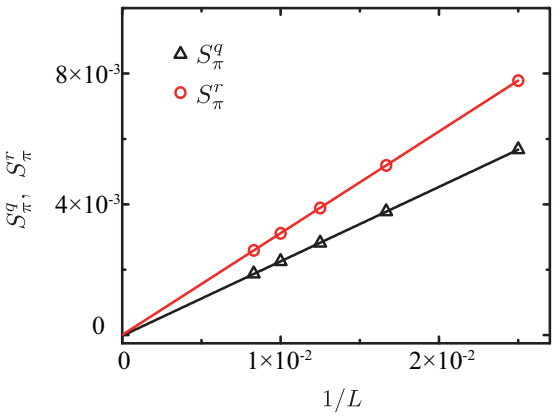

FIG. 6. The structure factors S_π^q and S_π^r versus $1/L$ at half filling with $g_l/2\pi = 55$ MHz and $g_r/2\pi = 245$ MHz.

that there is no crystalline or CDW ordered phases in this system at half filling [43].

C. Luttinger parameters

In the superfluid phase, the low-energy excitations of interacting bosons are effectively described by the Luttinger liquid Hamiltonian [72,73]

$$H_0 = \frac{1}{2\pi}\int ds\left[(v_\alpha K_\alpha)[\Pi_\alpha(x)]^2 + \left(\frac{v_\alpha}{K_\alpha}\right)[\partial_x\Phi_\alpha(x)]^2\right], \tag{37}$$

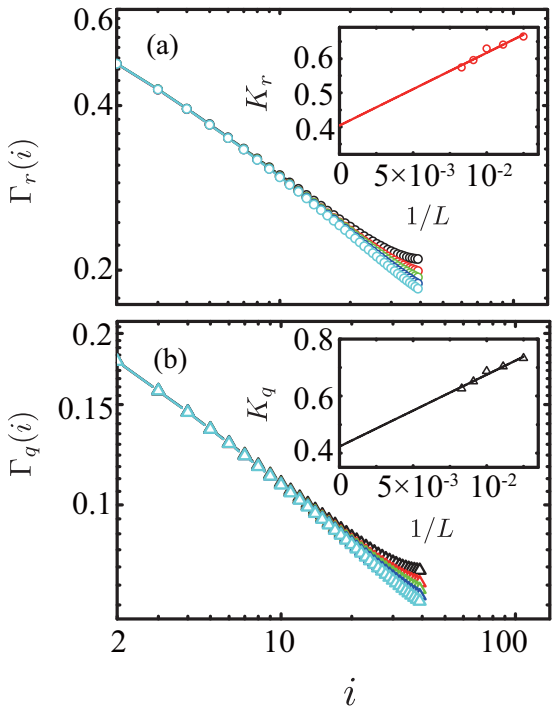

FIG. 7. The log-log plot of the single-particle density matrices $\Gamma_{q,r}(i)$ versus the distance i for the MCJC model at integer filling $N/L = 1$ with $g_{l,r}/2\pi = 150$ MHz. Insets: the Luttinger parameters $K_{q,r}$ versus $1/L$. The curves are for $L = 80,90,100,110,120$ from top to bottom.

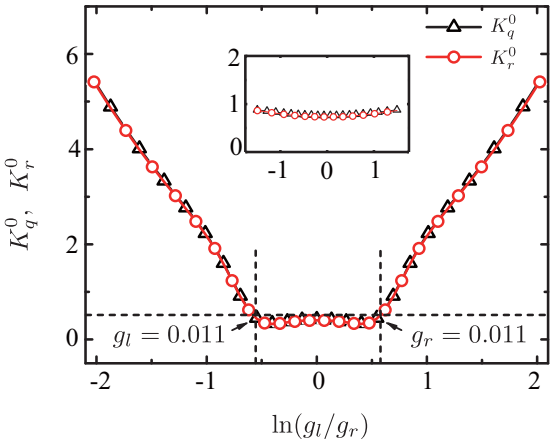

FIG. 8. The Luttinger parameters K_q^0 and K_r^0 versus $\ln(g_l/g_r)$ at $N/L = 1$ with $(g_r + g_l)/2\pi = 300$ MHz. The dashed horizontal line is $K_\alpha^0 = 1/2$. Inset: $K_{q,r}^0$ at $N/L = 1/2$.

where $\Phi_\alpha(x)$ $(\alpha = q,r)$ is the phase variable, $\Pi_\alpha(x)$ is the density fluctuation, v_α is the second sound velocity, and K_α is the Luttinger parameter that determines the exponents of the correlation functions in the large-distance limit with [77]

$$\Gamma_\alpha(i-j) \propto |i-j|^{-K_\alpha/2} \quad (\alpha = q,r). \tag{38}$$

Our calculation, as shown in Fig. 7, has indeed confirmed this power-law dependence for the single-particle density matrices. The deviation from the power-law dependence at large distance results from the finite-size effect. The power-law behaviors have also been observed at half filling, where the ground state is always in the SF phase. In contrast, in the MI phase, the single-particle density matrices decay exponentially with the distance.

The Luttinger parameters K_q and K_r are important parameters for characterizing the critical behavior of the MCJC model. To obtain the Luttinger parameters in the thermodynamic limit, an extrapolation of the finite-lattice results to the $L \to \infty$ limit is needed. From the numerical results, we find that K_α $(\alpha = q,r)$ can be well fitted by the formula (see the insets of Fig. 7)

$$K_\alpha = K_\alpha^0 + \lambda_\alpha/L, \tag{39}$$

where K_α^0 is the extrapolated Luttinger parameter in the limit $L \to \infty$ and λ_α is a coefficient.

The MI-SF phase transition at integer fillings is of the Kosterlitz-Thouless type, and $K_q^0 = K_r^0 = 1/2$ are expected at the critical points for $N/L = 1$ [43,72,73]. In contrast, the corresponding commensurate-incommensurate phase transitions satisfy $K_q^0 = K_r^0 = 1$. From the calculation of these Luttinger parameters, we can accurately determine the critical points. Figure 8 shows K_q^0 and K_r^0 as functions of $\ln(g_l/g_r)$ for the MCJC model at the integer filling $N/L = 1$. Within numerical accuracy, we find that $K_q^0 = K_r^0$ in the whole parameter range we have studied. Deep in the SF phase, $g_l \sim g_r$, $K_{q,r}^0 < 1/2$, indicating that the spatial correlation decreases slowly with the distance. As $|\ln(g_l/g_r)|$ is increased, $K_{q,r}^0$ increase and cross the points $K_{q,r}^0 = 1/2$ at $\beta_0 = g_l/g_r \approx 0.579$ and $1/\beta_0 = g_l/g_r \approx 1.727$. The Luttinger parameters at half filling, as shown in the inset of Fig. 8, are found to be $1/2 < K_\alpha^0 < 2$, indicating no phase transition in the whole parameter regime studied.

V. CONCLUSIONS

To conclude, we studied the ground-state properties of the 1D MCJC model of coupled qubits and cavities with the DMRG method. Using the polariton representation, we showed that the MCJC model is equivalent to the Bose-Hubbard model in the low-energy limit. From the numerical calculation, we determined accurately the phase boundaries, the correlation lengths, and the Luttinger parameters at both integer and half-integer fillings. Our result sheds light on the understanding of the critical behavior of strongly correlated polaritons in the MCJC lattice and related models.

ACKNOWLEDGMENTS

J.X. and T.X. are supported by the National Natural Science Foundation of China (Grants No. 11474331 and No. 11190024). K.S. and L.T. are supported by the National Science Foundation (USA) under Awards No. DMR-0956064 and No. PHY-1720501, the UC Multicampus-National Lab Collaborative Research and Training under Award No. LFR-17-477237, and UC Merced Faculty Research Grants 2017.

[1] M. H. Devoret and R. J. Schoelkopf, Science **339**, 1169 (2013).
[2] R. Blatt and C. F. Roos, Nat. Phys. **8**, 277 (2012).
[3] D. D. Awschalom, L. C. Bassett, A. S. Dzurak, E. L. Hu, and J. R. Petta, Science **339**, 1174 (2013).
[4] J. L. O'Brien, A. Furusawa, and J. Vučković, Nat. Photon. **3**, 687 (2009).
[5] G. Popkin, Science **354**, 1090 (2016).
[6] R. P. Feynman, Int. J. Theor. Phys. **21**, 467 (1982).
[7] S. Lloyd, Science **273**, 1073 (1996).
[8] P. Hauke, F. M. Cucchietti, L. Tagliacozzo, I. Deutsch, and M. Lewenstein, Rep. Prog. Phys. **75**, 082401 (2012).
[9] T. Langen, R. Geiger, and J. Schmiedmayer, Annu. Rev. Condens. Matter Phys. **6**, 201 (2015).
[10] I. Bloch, J. Dalibard, and S. Nascimbène, Nat. Phys. **8**, 267 (2012).
[11] D. S. Abrams and S. Lloyd, Phys. Rev. Lett. **79**, 2586 (1997).
[12] L.-A. Wu, M. S. Byrd, and D. A. Lidar, Phys. Rev. Lett. **89**, 057904 (2002).
[13] A. Aspuru-Guzik, A. D. Dutoi, P. J. Love, and M. Head-Gordon, Science **309**, 1704 (2005).
[14] P. J. J. O'Malley, R. Babbush, I. D. Kivlichan, J. Romero, J. R. McClean, R. Barends, J. Kelly, P. Roushan, A. Tranter, N. Ding, B. Campbell, Y. Chen, Z. Chen, B. Chiaro, A. Dunsworth, A. G. Fowler, E. Jeffrey, E. Lucero, A. Megrant, J. Y. Mutus, M. Neeley, C. Neill, C. Quintana, D. Sank, A. Vainsencher, J. Wenner, T. C. White, P. V. Coveney, P. J. Love, H. Neven,

A. Aspuru-Guzik, and J. M. Martinis, Phys. Rev. X **6**, 031007 (2016).
[15] S. Mostame, P. Rebentrost, A. Eisfeld, A. J. Kerman, D. I. Tsomokos, and A. Aspuru-Guzik, New J. Phys. **14**, 105013 (2012).
[16] V. M. Stojanović, T. Shi, C. Bruder, and J. I. Cirac, Phys. Rev. Lett. **109**, 250501 (2012).
[17] F. Mei, V. M. Stojanović, I. Siddiqi, and L. Tian, Phys. Rev. B **88**, 224502 (2013).
[18] V. M. Stojanović, M. Vanević, E. Demler, and L. Tian, Phys. Rev. B **89**, 144508 (2014).
[19] M. W. Johnson, M. H. S. Amin, S. Gildert, T. Lanting, F. Hamze, N. Dickson, R. Harris, A. J. Berkley, J. Johansson, P. Bunyk, E. M. Chapple, C. Enderud, J. P. Hilton, K. Karimi, E. Ladizinsky, N. Ladizinsky, T. Oh, I. Perminov, C. Rich, M. C. Thom, E. Tolkacheva, C. J. S. Truncik, S. Uchaikin, J. Wang, B. Wilson, and G. Rose, Nature (London) **473**, 194 (2011).
[20] S. Boixo, T. F. Rønnow, S. V. Isakov, Z. Wang, D. Wecker, D. A. Lidar, J. M. Martinis, and M. Troyer, Nat. Phys. **10**, 218 (2014).
[21] L. Tian, Phys. Rev. Lett. **105**, 167001 (2010).
[22] U. L. Heras, A. Mezzacapo, L. Lamata, S. Filipp, A. Wallraff, and E. Solano, Phys. Rev. Lett. **112**, 200501 (2014).
[23] R. Barends, A. Shabani, L. Lamata, J. Kelly, A. Mezzacapo, U. L. Heras, R. Babbush, A. G. Fowler, B. Campbell, Y. Chen, Z. Chen, B. Chiaro, A. Dunsworth, E. Jeffrey, E. Lucero, A. Megrant, J. Y. Mutus, M. Neeley, C. Neill, P. J. J. O'Malley, C. Quintana, P. Roushan, D. Sank, A. Vainsencher, J. Wenner, T. C. White, E. Solano, H. Neven, and J. M. Martinis, Nature (London) **534**, 222 (2016).
[24] E. Kapit, Phys. Rev. A **87**, 062336 (2013).
[25] D. Marcos, P. Rabl, E. Rico, and P. Zoller, Phys. Rev. Lett. **111**, 110504 (2013).
[26] B. Peropadre, D. Zueco, F. Wulschner, F. Deppe, A. Marx, R. Gross, and J. J. García-Ripoll, Phys. Rev. B **87**, 134504 (2013).
[27] R. Landig, L. Hruby, N. Dogra, M. Landini, R. Mottl, T. Donner, and T. Esslinger, Nature (London) **532**, 476 (2015).
[28] J. Klinder, H. Keßler, M. R. Bakhtiari, M. Thorwart, and A. Hemmerich, Phys. Rev. Lett. **115**, 230403 (2015).
[29] J. Léonard, A. Morales, P. Zupancic, T. Esslinger, and T. Donner, Nature (London) **543**, 87 (2017).
[30] I. B. Mekhov and H. Ritsch, J. Phys. B **45**, 102001 (2012).
[31] H. Ritsch, P. Domokos, F. Brennecke, and T. Esslinger, Rev. Mod. Phys. **85**, 553 (2013).
[32] S. F. Caballero-Benitez and I. B. Mekhov, Phys. Rev. Lett. **115**, 243604 (2015).
[33] S. F. Caballero-Benitez, G. Mazzucchi, and I. B. Mekhov, Phys. Rev. A **93**, 063632 (2016).
[34] P. Strack and S. Sachdev, Phys. Rev. Lett. **107**, 277202 (2011).
[35] S. Gopalakrishnan, B. S. Lev, and P. M. Goldbart, Nat. Phys. **5**, 845 (2009).
[36] M. J. Hartmann, F. Brandão, and M. Plenio, Laser Photon. Rev. **2**, 527 (2008).
[37] A. A. Houck, H. E. Türeci, and J. Koch, Nat. Phys. **8**, 292 (2012).
[38] M. J. Hartmann, F. G. S. L. Brandão, and M. B. Plenio, Nat. Phys. **2**, 849 (2006).
[39] A. D. Greentree, C. Tahan, J. H. Cole, and L. C. L. Hollenberg, Nat. Phys. **2**, 856 (2006).
[40] D. G. Angelakis, M. F. Santos, and S. Bose, Phys. Rev. A **76**, 031805(R) (2007).
[41] M. P. A. Fisher, P. B. Weichman, G. Grinstein, and D. S. Fisher, Phys. Rev. B **40**, 546 (1989).
[42] G. G. Batrouni, R. T. Scalettar, and G. T. Zimanyi, Phys. Rev. Lett. **65**, 1765 (1990).
[43] T. D. Kühner and H. Monien, Phys. Rev. B **58**, R14741(R) (1998).
[44] T. D. Kühner, S. R. White, and H. Monien, Phys. Rev. B **61**, 12474 (2000).
[45] D. Rossini and R. Fazio, Phys. Rev. Lett. **99**, 186401 (2007).
[46] N. Na, S. Utsunomiya, L. Tian, and Y. Yamamoto, Phys. Rev. A **77**, 031803(R) (2008).
[47] M. I. Makin, J. H. Cole, C. Tahan, L. C. L. Hollenberg, and A. D. Greentree, Phys. Rev. A **77**, 053819 (2008).
[48] S. Schmidt and G. Blatter, Phys. Rev. Lett. **103**, 086403 (2009).
[49] J. Koch and K. Le Hur, Phys. Rev. A **80**, 023811 (2009).
[50] P. Pippan, H. G. Evertz, and M. Hohenadler, Phys. Rev. A **80**, 033612 (2009).
[51] A. L. C. Hayward, A. M. Martin, and A. D. Greentree, Phys. Rev. Lett. **108**, 223602 (2012).
[52] A. G. D'Souza, B. C. Sanders, and D. L. Feder, Phys. Rev. A **88**, 063801 (2013).
[53] S. J. Srinivasan, A. J. Hoffman, J. M. Gambetta, and A. A. Houck, Phys. Rev. Lett. **106**, 083601 (2011).
[54] A. J. Hoffman, S. J. Srinivasan, S. Schmidt, L. Spietz, J. Aumentado, H. E. Türeci, and A. A. Houck, Phys. Rev. Lett. **107**, 053602 (2011).
[55] F. Nissen, S. Schmidt, M. Biondi, G. Blatter, H. E. Türeci, and J. Keeling, Phys. Rev. Lett. **108**, 233603 (2012).
[56] M. Fitzpatrick, N. M. Sundaresan, A. C. Y. Li, J. Koch, and A. A. Houck, Phys. Rev. X **7**, 011016 (2017).
[57] K. Seo and L. Tian, Phys. Rev. B **91**, 195439 (2015).
[58] K. Seo and L. Tian, Sci. China-Phys. Mech. Astron. **58**, 070302 (2015).
[59] Y. Qiu, W. Xiong, L. Tian, and J. Q. You, Phys. Rev. A **89**, 042321 (2014).
[60] A. Kurcz, A. Bermudez, and J. J. García-Ripoll, Phys. Rev. Lett. **112**, 180405 (2014).
[61] R. Barends, J. Kelly, A. Megrant, D. Sank, E. Jeffrey, Y. Chen, Y. Yin, B. Chiaro, J. Mutus, C. Neill, P. O'Malley, P. Roushan, J. Wenner, T. C. White, A. N. Cleland, and J. M. Martinis, Phys. Rev. Lett. **111**, 080502 (2013).
[62] Y. Chen, C. Neill, P. Roushan, N. Leung, M. Fang, R. Barends, J. Kelly, B. Campbell, Z. Chen, B. Chiaro, A. Dunsworth, E. Jeffrey, A. Megrant, J. Y. Mutus, P. J. J. O'Malley, C. M. Quintana, D. Sank, A. Vainsencher, J. Wenner, T. C. White, M. R. Geller, A. N. Cleland, and J. M. Martinis, Phys. Rev. Lett. **113**, 220502 (2014).
[63] S. R. White, Phys. Rev. Lett. **69**, 2863 (1992).
[64] S. R. White, Phys. Rev. B **48**, 10345 (1993).
[65] S. Sachdev, *Quantum Phase Transitions* (Cambridge University Press, Cambridge, 1999).
[66] J. Majer, J. M. Chow, J. M. Gambetta, J. Koch, B. R. Johnson, J. A. Schreier, L. Frunzio, D. I. Schuster, A. A. Houck, A. Wallraff, A. Blais, M. H. Devoret, S. M. Girvin, and R. J. Schoelkopf, Nature (London) **449**, 443 (2007).
[67] M. Hofheinz, H. Wang, M. Ansmann, R. C. Bialczak, E. Lucero, M. Neeley, A. D. O'Connell, D. Sank, J. Wenner, J. M. Martinis, and A. N. Cleland, Nature (London) **459**, 546 (2009).
[68] E. Jaynes and F. Cummings, Proc. IEEE **51**, 89 (1963).

[69] J. M. Raimond, M. Brune, and S. Haroche, Rev. Mod. Phys. **73**, 565 (2001).
[70] S. M. Girvin, *Strong Light-Matter Coupling: From Atoms to Solid-State Systems* (World Scientific, Singapore, 2014), pp. 155–206.
[71] J. Q. You and F. Nori, Nature (London) **474**, 589 (2011).
[72] J. M. Kosterlitz and D. J. Thouless, J. Phys. C **6**, 1181 (1973).
[73] J. M. Kosterlitz, J. Phys. C **7**, 1046 (1974).
[74] U. Schollwöck, Ann. Phys. (NY) **326**, 96 (2011).
[75] O. Penrose and L. Onsager, Phys. Rev. **104**, 576 (1956).
[76] C. N. Yang, Rev. Mod. Phys. **34**, 694 (1962).
[77] F. D. M. Haldane, Phys. Rev. Lett. **47**, 1840 (1981).